tight junctions are critical for restricting paracellular diffusion in the cerebral microvasculature. Increased cerebrovascular permeability is a principal factor in the development of cerebral edema after brain ischemia. Several studies have shown a relationship between cyclic AMP (cAMP) levels and permeability of endothelial cell monolayers. For example, elevation of intracellular cAMP concentrations induces high transendothelial electrical resistance and increases P-glycoprotein function in brain capillary endothelial cells (11, 12). In addition, when bovine aortic endothelial cells were cultured in hypoxic conditions, cellular cAMP levels decreased and this phenomenon was associated with an increase in cellular permeability (13). Furthermore, a decrease in cAMP levels was detectable after brain microvascular endothelial cells were exposed to hypoxic conditions for 3 h (14). Moreover, indapamide was shown to augment cAMP production induced by forskolin, an adenylyl cyclase activator, but did not alter basal cAMP levels in cardiomyocytes alone. (15). Therefore, indapamide may protect cerebral microvascular endothelial cells from ischemic dysfunction by increasing intracellular cAMP levels. The effects of indapamide on the expression of tight junction-related proteins and on intracellular messengers are now being investigated in rat brain primary cultured endothelial cells.

We present here in vitro evidence to suggest a possible protective action of

indapamide against ischemia/reperfusion-induced injury and dysfunction of the BBB.

Acknowledgements

Indapamide was kindly provided from Kyoto pharmaceutical industries Co., Ltd. This work was supported, in part, by Grants-in-Aid for Scientific Research ((B) 17390159) from JSPS, Japan and by a research fund from Fukuoka University (No. 003171PK, Sumitomo Pharma Co., Ltd).

References

1 Partridge W.M. Blood–brain barrier biology and methodology. J. Neurovirology. 1999;5: 556–569.

2 Mark KS, Davis TP. Cerebral microvascular changes in permeability and tight junctions induced by hypoxia-reoxygenation. Am J Physiol Heart Circ Physiol. 2002;282:H1485-H1494.

3 Hayashi K, Nakao S, Nakaoke R, Nakagawa S, Kitagawa N, Niwa M. Effects of hypoxia on endothelial/pericytic co-culture model of the blood-brain barrier. Regul Pept. 2004;123:77-83.

4 Brown R.C. and Davis T.P. Calcium modulation of adherens and tight junction function: a potential mechanism for blood–brain barrier disruption after stroke. Stroke 2002;33:1706–1711.

5 O'Donnell M.E., Tran L., Lam T.I., Liu X.B. and Anderson S.E. Bumetanide inhibition of the blood–brain barrier Na–K–Cl cotransporter reduces edema formation in the rat middle cerebral artery occlusion model of stroke, J. Cereb. Blood Flow Metab. 2004;24:1046–1056.

6 Boucher FR, Schatz CJ, Guez DM, de Leiris JG. Beneficial effect of indapamide in experimental myocardial ischemia. Am J Hypertens. 1992;5:22-25.

7 PROGRESS Collaborative Group. Randomised trial of a perindopril-based blood-pressure-lowering regimen among 6,105 individuals with previous stroke or transient ischaemic attack. Lancet. 2001;358:1033-1041.

8 Tatsuta T., Naito M., Oh-hara T., Sugawara I. and Tsuruo T., Functional involvement of P-glycoprotein in blood–brain barrier, J. Biol. Chem. 1992;267:20383–20391.

9 Dohgu S, Yamauchi A, Takata F, Naito M, Tsuruo T, Higuchi S, et al. Transforming growth factor-beta1 upregulates the tight junction and P-glycoprotein of brain microvascular endothelial cells. Cell Mol Neurobiol. 2004;24:491-497.

10 Dehouck MP, Jolliet-Riant P, Bree F, Fruchart JC, Cecchelli R, Tillement JP. Drug transfer across the blood–brain barrier: correlation between in vitro and in vivo models. J. Neurochem. 1992;58:1790–1797.

11 Kis B, Deli MA, Kobayashi H, Abraham CS, Yanagita T, Kaiya H, et al. Adrenomedullin regulates blood-brain barrier functions in vitro. Neuroreport. 2001;12:4139-4142.

12 Deli MA, Abraham CS, Takahata H, Niwa M. Tissue plasminogen activator inhibits P-glycoprotein activity in brain endothelial cells. Eur J Pharmacol. 2001;411:R3-R5.

13 Ogawa S, Koga S, Kuwabara K, Brett J, Morrow B, Morris SA, et al. Hypoxia-induced increased permeability of endothelial monolayers occurs through

lowering of cellular cAMP levels. Am J Physiol. 1992;262:C546-554.

14 Fischer S, Renz D, Schaper W, Karliczek GF. Effects of barbiturates on hypoxic cultures of brain derived microvascular endothelial cells. Brain Res. 1996;707:47-53.

15 Rabkin SW. Indapamide alters the cyclic AMP signal transduction pathway in cardiomyocytes in culture. Eur J Pharmacol. 1994;266:117-123.

Figure legends

Fig. 1. Effects of indapamide on the viability of MBEC4 cells subjected to normal (A) or ischemia/reperfusion (B) conditions. Results are expressed as % of cell viability under normal conditions with vehicle treatment (% of vehicle). The % recovery is shown on the right-side of panel B and was calculated using the following equation: [% of vehicle under ischemia/reperfusion conditions with indapamide treatment - % of vehicle under ischemia/reperfusion conditions with vehicle treatment] / [% of vehicle under normal conditions with vehicle treatment - % of vehicle under ischemia/reperfusion conditions with vehicle treatment] x 100. Data are expressed as mean ± S.E.M. (n=8-20). ## $p<0.01$, significant difference from vehicle under normal conditions. **$p<0.01$, significant difference from vehicle under ischemia/reperfusion conditions.

Fig. 2. Effects of indapamide on Na-F (A) and EBA (B) permeability in MBEC4 cell monolayer after a 7 h exposure to normal or ischemia conditions. The inset in each panel shows the effects of indapamide on permeability of the MBEC4 cell monolayer to Na-F and EBA after a 7 h exposure to normal conditions. The permeability coefficients of Na-F and EBA in the MBEC4 monolayer, after a 7 h exposure to normal conditions with vehicle treatment, were $3.109 \pm 0.012 \times 10^{-4}$ and $0.798 \pm 0.003 \times 10^{-4}$ cm/min,

respectively. Results are expressed as % of vehicle under normal conditions with vehicle treatment. The % recovery is shown on the right-side of each panel and was calculated by the following equation: [% of vehicle under ischemia condition with indapamide treatment - % of vehicle under ischemia condition with vehicle treatment] / [% of vehicle under normal condition with vehicle treatment - % of vehicle under ischemia condition with vehicle treatment] x 100. Data are expressed as mean ± S.E.M. (n=8). ##$p<0.01$, significant difference from vehicle under normal conditions. **$p<0.01$, significant difference from vehicle under ischemia conditions.

Fig. 1 (Nishioku et al)

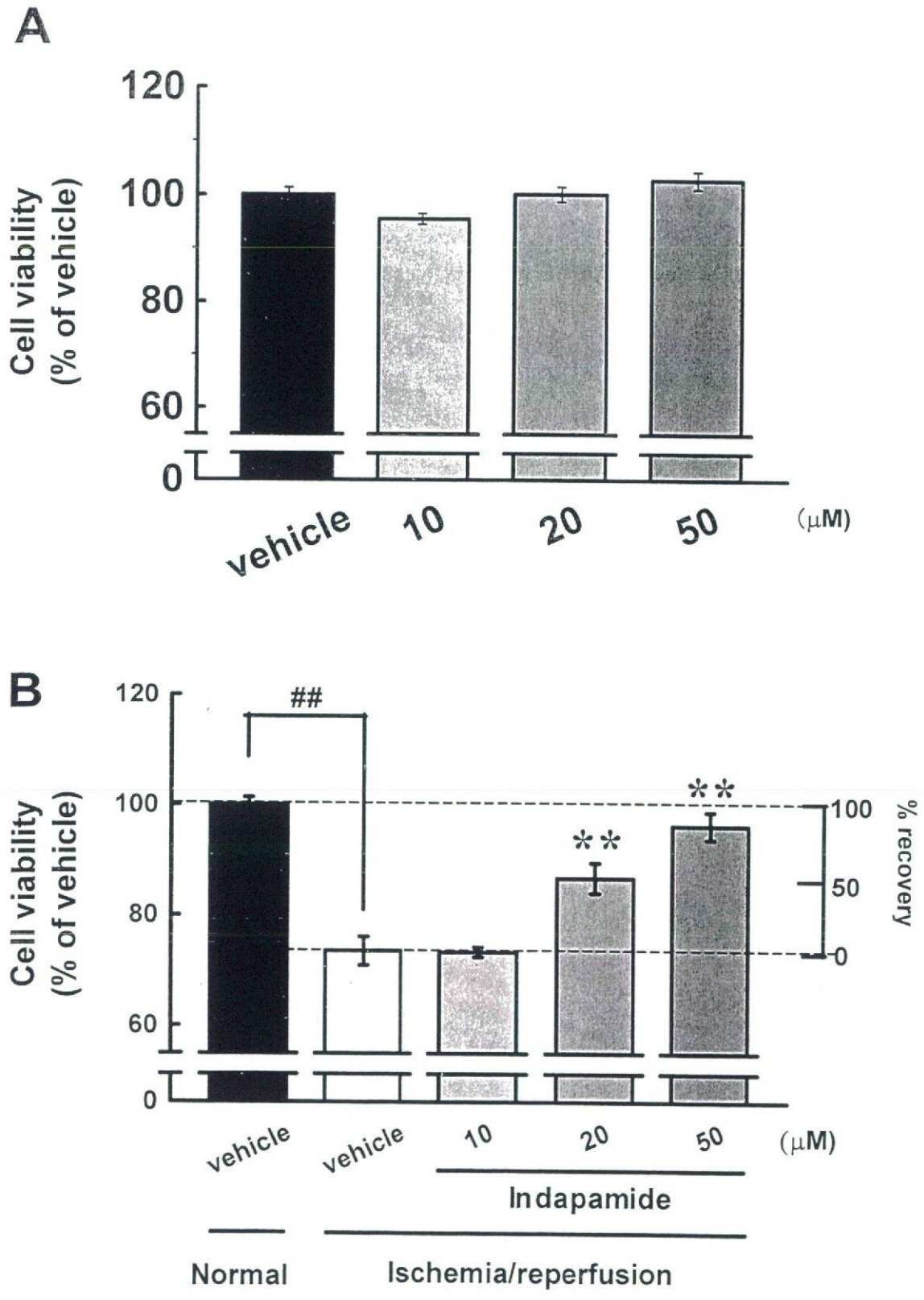

Fig. 2 (Nishioku et al)

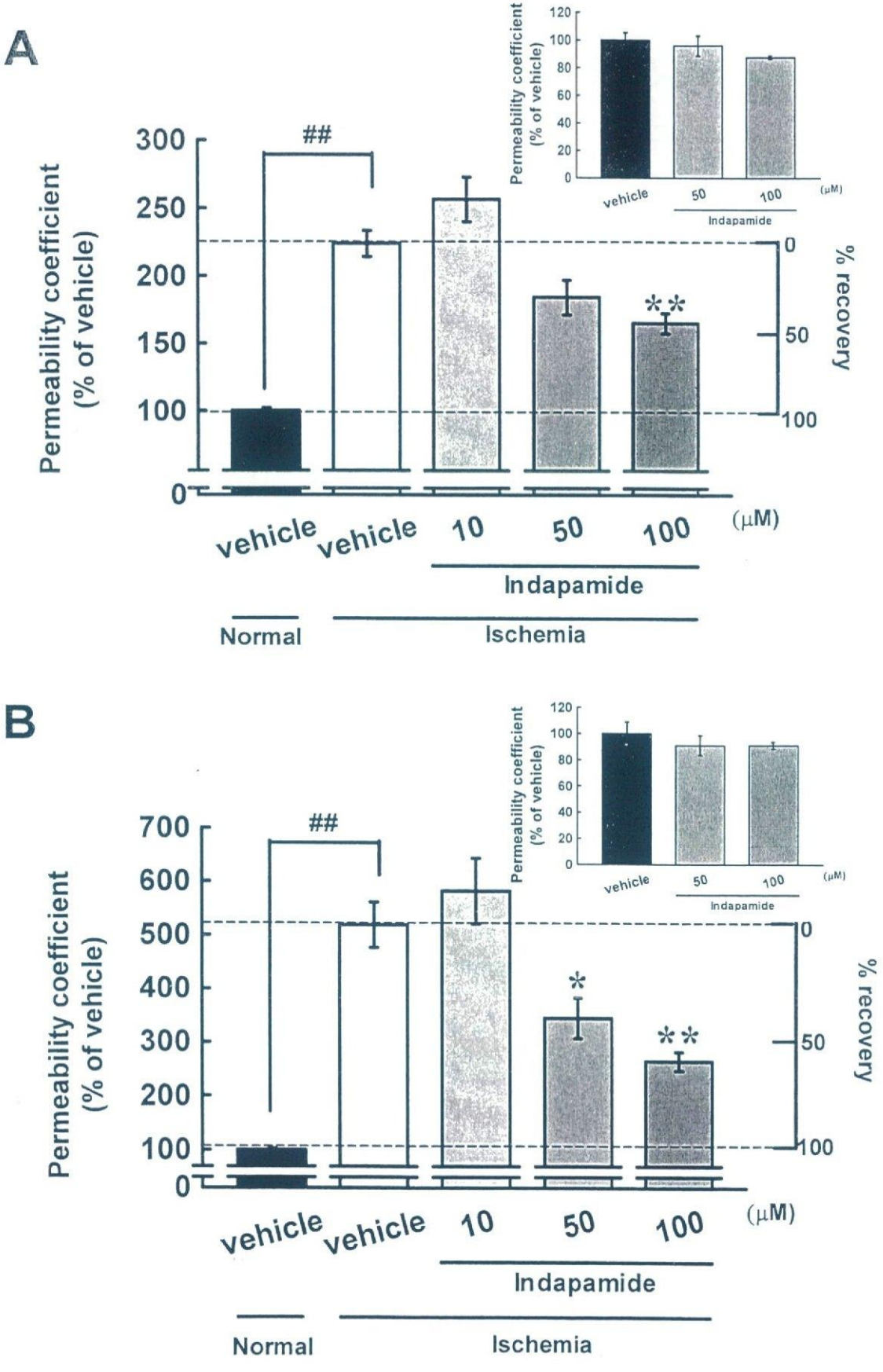

0022-3565/06/3162-647–653$20.00
THE JOURNAL OF PHARMACOLOGY AND EXPERIMENTAL THERAPEUTICS

JPET 316:647–653, 2006

Vol. 316, No. 2
88328/3082565
Printed in U.S.A.

In Vivo Evaluation of P-glycoprotein Function at the Blood-Brain Barrier in Nonhuman Primates Using [^{11}C]Verapamil

Young-Joo Lee,[1] Jun Maeda, Hiroyuki Kusuhara, Takashi Okauchi, Motoki Inaji, Yuji Nagai, Shigeru Obayashi, Ryuji Nakao, Kazutoshi Suzuki, Yuichi Sugiyama, and Tetsuya Suhara

The Graduate School of Pharmaceutical Sciences, the University of Tokyo, Bunkyo-ku, Tokyo, Japan (Y.-J. L., H.K., Y.S.); Brain Imaging Project, National Institute of Radiological Sciences, Chiba, Japan (J.M., T.O., M.I., Y.N., S.O., T.S.); and Department of Medical Imaging, National Institute of Radiological Sciences, Chiba, Japan (R.N., K.S.)

Received April 21, 2005; accepted November 16, 2005

ABSTRACT

P-glycoprotein (P-gp) is a major efflux transporter contributing to the efflux of a range of xenobiotic compounds at the blood-brain barrier (BBB). In the present study, we evaluated the P-gp function at the BBB using positron emission tomography (PET) in nonhuman primates. Serial brain PET scans were obtained in three rhesus monkeys after intravenous administration of [^{11}C]verapamil under control and P-gp inhibition conditions ([PSC833 ([3′-keto-Me-Bmt^1]-[Val^2]-cyclosporin) 20 mg/kg/2 h]). The parent [^{11}C]verapamil and its metabolites in plasma were determined by HPLC with a positron detector. The initial brain uptake clearance calculated from the integration plot was used for the quantitative analysis. After intravenous administration, [^{11}C]verapamil was taken up rapidly into the brain (time to reach the peak, 0.58 min). The blood level of [^{11}C]verapamil decreased rapidly, and it underwent metabolism with time. The inhibition of P-gp by PSC833 increased the brain uptake of [^{11}C]verapamil 4.61-fold (0.141 versus 0.651 ml/g brain/min, $p < 0.05$). These results suggest that PET measurement with [^{11}C]verapamil can be used for the evaluation of P-gp function at the BBB in the living brain.

The blood-brain barrier (BBB), formed by brain-capillary endothelial cells, is a functional barrier responsible for restricting the entry of compounds from the circulating blood to the brain parenchyma cells (Reese and Karnovsky, 1967). The highly developed tight junctions between the adjacent brain cerebral endothelial cells are an anatomical feature of the BBB that minimizes the nonspecific penetration of compounds via paracellular route (Pardridge, 1988). In addition to this physical barrier, metabolic enzymes and active efflux transporters on this barrier also play important roles in BBB function. P-glycoprotein (P-gp), a 170-kDa membrane protein that is responsible for the multidrug resistance of tumor cells, is a major efflux transporter contributing to the efflux of a range of xenobiotic compounds in the circulating blood at the BBB (Schinkel et al., 1994; Tamai and Tsuji, 2000; Kusuhara and Sugiyama, 2001; Hirrlinger et al., 2002). Interestingly, P-gp may also be involved in the efflux of β-amyloid and has been suspected to play a role in Alzheimer's disease (Lam et al., 2001; Vogelgesang et al., 2002). In addition, a drug-drug interaction involving P-gp inhibition at the BBB has also been suggested (Sadeque at al., 2000). In a clinical study, when loperamide was administered with quinidine, a known P-gp inhibitor, respiratory depression by loperamide was induced (Sadeque at al., 2000). It is speculated that this is caused by modulation of the P-gp-mediated efflux by quinidine. Furthermore, a genetic polymorphism (C3435T) of P-gp has been reported to be associated with drug resistance in patients with epilepsy (Siddiqui et al., 2003), although a controversial result was reported recently (Tan et al., 2004). Such a genetic polymorphism may be associated with interindividual differences in drug concentration in the central nervous system.

This study was performed through the Advanced and Innovational Research program in Life Sciences from the Ministry of Education, Culture, Sports, Science and Technology, Japan. This work was also partially supported by a research grant from the Society of Japanese Pharmacopoeia and the Minister of Health, Labor and Welfare.

[1] Current affiliation: College of Pharmacy, Kyung Hee University, Seoul, Korea.

Article, publication date, and citation information can be found at http://jpet.aspetjournals.org.
doi:10.1124/jpet.105.088328.

ABBREVIATIONS: BBB, blood-brain barrier; ANOVA, analysis of variance; AUC, area under the curve; C_{max}, maximal concentration; HPLC, high-pressure liquid chromatography; MRI, magnetic resonance image; PET, positron emission tomography; P-gp, P-glycoprotein; PSC833, [3′-keto-Me-Bmt^1]-[Val^2]-cyclosporin; T_{max}, time to reach the C_{max}.

These clinical reports prompted a growing interest in the quantitative evaluation of P-gp function in living human brain.

Recently, in vivo evaluation of P-gp function was proposed using an imaging method with [^{11}C]colchicine, [^{11}C]carvedilol, [^{18}F]paclitaxel, and [^{11}C]verapamil (Elsinga et al., 2004). Hendrikse et al. (1998) demonstrated in rodents that the brain uptake of the P-gp substrate [^{11}C]verapamil was increased after pretreatment with cyclosporin A, a P-gp inhibitor, and they showed that that the distribution volume, estimated by Logan plot, was increased by pretreatment with cyclosporin A (Bart et al., 2003; Elsinga et al., 2004). As for human studies, Sasongko et al. (2005) demonstrated that the ratio of the area under the curve (AUC) of the brain concentration to that of blood concentration was increased in the presence of cyclosporin A, and Kortekaas et al. (2005) reported that the distribution volume of [^{11}C]verapamil in the midbrain was increased in Parkinson's disease patients compared with controls. In the present study, the P-gp function at the BBB was evaluated in rhesus monkeys by PET using [^{11}C]verapamil, with or without a potent P-gp inhibitor PSC833. PSC833 treatment caused a significant increase in the brain uptake clearance of [^{11}C]verapamil, which was determined using integration plot analysis using initial brain and blood concentration data.

Materials and Methods

Chemicals. The P-gp inhibitor PSC833 (Valspodar) was kindly supplied by Novartis (Basel, Switzerland) and was dissolved in Intralipid (Lo et al., 2001) (oil in water emulsion droplet; Otsuka Pharmaceutical, Tokyo, Japan). [^{11}C]Verapamil was synthesized from norverapamil (Eisai Co. Ltd., Tokyo, Japan) as described previously (Wegman et al., 2002) and diluted with approximately 2 to 3 ml 0.9% saline containing 0.75% polyoxyethylenemonosorbitan oleate and 1% ascorbic acid. The specific radioactivity of [^{11}C]verapamil used in all experiments ranged from 28.3 to 79.7 GBq/μmol (47.6 ± 17.3 GBq/μmol, mean ± S.D., radiochemical purity is over 95%).

Animals. Three young male rhesus monkeys (Macaca mulatta) weighing approximately 6.0 to 6.7 kg were used. The monkeys were maintained and handled in accordance with recommendations by the United States National Institutes of Health and our own guidelines (National Institute of Radiological Sciences, Chiba, Japan). The study was approved by the Animal Ethics Committee of the National Institute of Radiological Sciences. A magnetic resonance image (MRI) of each monkey brain was obtained beforehand.

PET Scan. All PET scans were performed using a high-resolution SHR-7700 PET camera (Hamamatsu Photonics, Shizuoka, Japan) designed for laboratory animals, which provides 31 transaxial slices 3.6 mm (center-to-center) apart, a 33.1-cm field of view, and spatial resolution of 2.6 mm full width at half-maximum (Watanabe et al., 1997). Monkeys were trained beforehand as being immobilized with the head fixation device to ensure accuracy of repositioning throughout the session (Obayashi et al., 2001). The infusion of PSC833 (20 mg/kg/2 h), a P-gp modulator, or vehicle alone to each monkey was started 1 h before the intravenous administration of [^{11}C]verapamil and maintained during the experiment. After administration of [^{11}C]verapamil, 0.9% saline was flushed into the catheter line to prevent adsorption or retention of verapamil. Arterial blood sampling (~0.5–1.5 ml) was performed via an indwelling arterial port from the saphenous artery at 10 s, 20 s, 30 s, 45 s, 1 min, 1.5 min, 3 min, 4.5 min, 6 min, 8 min, 10 min, 15 min, 20 min, 30 min, 45 min, and 60 min after administration, and the radioactivity in the blood was counted in a well-type γ-scintillation counter. Radioactivity was corrected for decay. After transmission scans for attenuation correction for 30 min, a dynamic emission scan in enhanced 2D mode was performed for 60 min (10 × 12 s, 30 × 6 s, 1 × 5 min, 2 × 5 min, and 5 × 8 min; a total of 36 frames). [^{11}C]Verapamil was administered via the saphenous vein as a single bolus at the start of the emission scan. The injected doses of [^{11}C]verapamil were 65.8 ± 11.5 MBq/kg (mean ± S.D.). The PET scans were separated by at least 4-week intervals and randomized for each monkey.

Metabolite Analysis. Arterial blood samples were collected at 1, 3, 6, 10, 15, 30, and 60 min after administration of [^{11}C]verapamil. Plasma was obtained by centrifugation and deproteinized with 2 volumes of acetonitrile. The supernatant was analyzed for radioactive components using a high-pressure liquid chromatography (HPLC) system (PU-610A series; GL Sciences, Torrance, CA) with a coupled NaI(Tl) positron detector (Takei et al., 2001) to measure [^{11}C]verapamil metabolites. Isocratic elution was performed with a reversed-phase semipreparative μ-Bondpak C18 column (7.8 × 300 mm i.d.; Waters, Milford, MA). The mobile phase consisted of a mixture of acetonitrile and 0.1 M ammonium acetate (70:30 v/v). The flow rate was 5 ml/min, and the injected sample size was 1.0 ml. The elute was monitored by ultraviolet absorbance at 254 nm and coupled NaI(Tl) positron detection. The percentage of parent radioactivity was determined from the activity of the parent verapamil with respect to the ^{11}C radioactivity in the chromatogram.

PET Data Analysis. All emission scan images were reconstructed with a 4.0-mm Hann filter, and regions of interest were placed on the whole cerebrum using PET Analyzer (in-house software, National Institute of Radiological Sciences; Maeda et al., 2001), and MRI information on each monkey. The summation images of [^{11}C]verapamil from 0 to 5 min were coregistered on the magnetic resonance images by means of statistical parametric mapping (SPM 2; Welcome Department of Cognitive Neurology, London, UK), and then the volume images were processed with Virtual Place TM (AZE Ltd. Tokyo, Japan). The decay-corrected ^{11}C radioactivity was normalized to the injected dose (% dose). The maximal ^{11}C radioactivity in the cerebrum (C_{max_cereb}) and the time to reach the C_{max_cereb} (T_{max_cereb}) were obtained from the time-^{11}C radioactivity data. The AUC was calculated for brain and blood, and it was calculated using data from 0 to 4.5 min after administration to minimize the bias by metabolites.

Integration Plot. The initial brain uptake was measured over a short period (~1–4.5 min) using integration plot method. The uptake rate of [^{11}C]verapamil can be described by the following equation,

$$\frac{X_{t,cereb}}{C_{t,blood}} = CL_{uptake} \times \frac{AUC_{(0-t)}}{C_{t,blood}} + V_E \qquad (1)$$

where CL_{uptake} is the brain uptake clearance based on the blood ^{11}C radioactivity, $X_{t,cereb}$ is the amount of ^{11}C radioactivity in the cerebrum at time t, and $C_{t,blood}$ is the blood concentration calculated from ^{11}C radioactivity. $AUC_{(0-t)}$ represents the area under the blood concentration curve from 0 to t, and V_E represents the initial distribution volume in the brain at time 0. V_E was obtained from the y-intercept of the integration plot and includes the distribution volume in blood residing within the brain as well as the initial distribution volume of [^{11}C]verapamil in the brain rapidly equilibrating with that in blood. Therefore, the CL_{uptake} value can be obtained from the initial slope of a plot of $X_{t,cereb}/C_{t,blood}$ versus $AUC_{(0-t)}/C_{t,blood}$, designated as the integration plot (Kim et al., 1988).

Inhibition of P-gp Function. The effect of PSC833, a P-gp modulator, was evaluated based on the normalized time-activity curves of brain and blood for the three monkeys, with and without PSC833 administration. PSC833 was infused at a dose of 20 mg/kg/2 h starting 1 h before intravenous administration of [^{11}C]verapamil and maintained until the end of the experiment (Song et al., 1999; Rodriguez et al., 2004). In a control experiment, drug vehicle was infused in the same manner. Differences were considered statistically significant when $p < 0.05$ using a one-sided paired t test, with the exception of the time course results in which two-way analysis of variance was used.

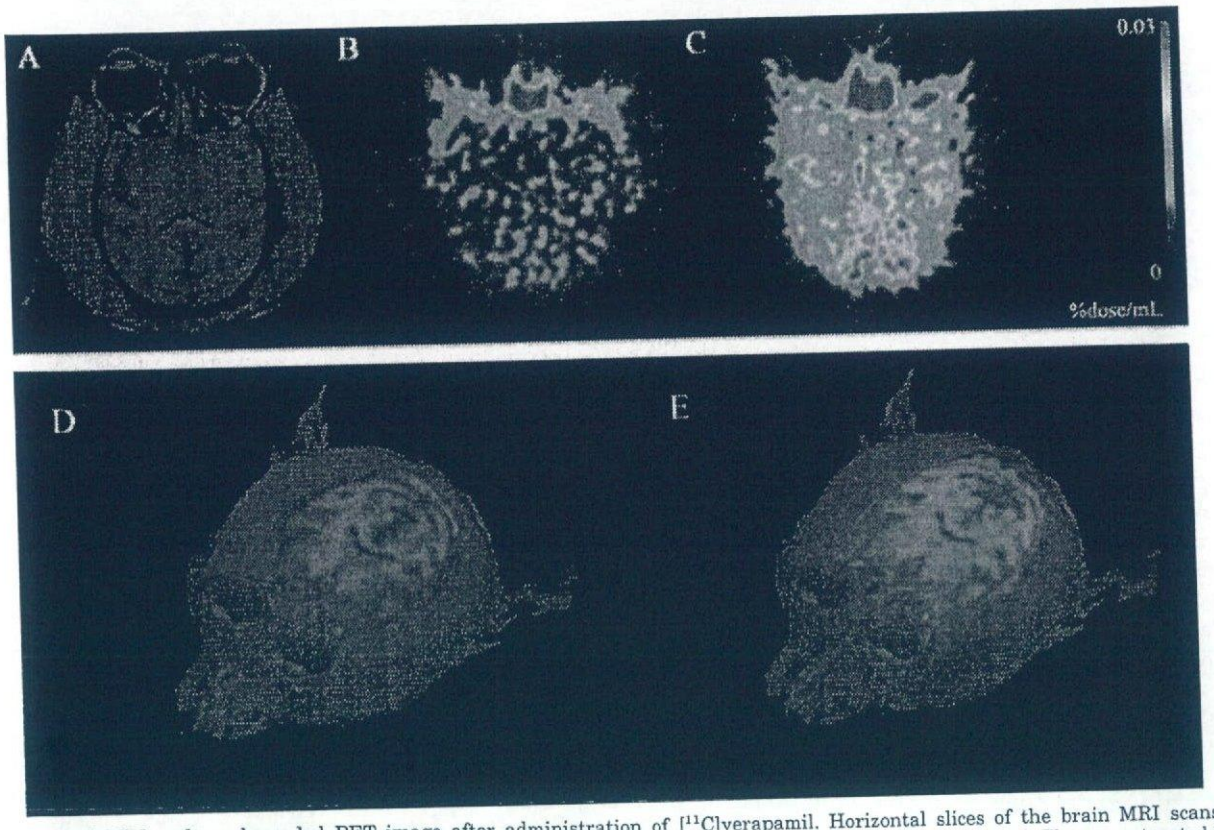

Fig. 1. A typical MRI and a color-coded PET image after administration of [^{11}C]verapamil. Horizontal slices of the brain MRI scans (A) and corresponding summation of PET images (B and C, up to 5 min) of the cerebral ^{11}C radioactivity uptake in one animal. The reconstructed MRI-PET image is also shown to assist intuitive understanding (D and E). B and D represent the control state, and C and E are the P-gp inhibition conditions obtained after PSC833 administration.

Results

The Distribution of [^{11}C]Verapamil in the Brain. A control PET image (Fig. 1B) accompanied by a corresponding morphological MRI (Fig. 1A) showed the uptake of ^{11}C radioactivity in the monkey brain. Higher uptake of ^{11}C radioactivity was observed in the brain after PSC833 treatment (Fig. 1C, PSC833-treated). Brain uptake was also clearly identified from PET/MRI-coregistered images (Fig. 1, D and E). The time-activity curves in the cerebrum are shown in Fig. 2. The ^{11}C radioactivity in the cerebrum peaked at 0.58 min after intravenous administration of [^{11}C]verapamil and remained almost constant at this level up to 60 min. Only limited amount of ^{11}C radioactivity (0.0105 ± 0.0006% dose/g brain, C_{max_cereb}, mean ± S.D.) was transported into the cerebrum.

Treatment with PSC833 significantly increased the ^{11}C radioactivity uptake in the cerebrum (two-way ANOVA, $p < 0.05$). The cerebrum AUC (AUC_{cereb}) of the PSC833 treatment group was significantly greater than that of the control group (1.96-fold) (Table 1; $p < 0.05$). The C_{max_cereb} of the PSC833 treatment group was also significantly higher than that of the control group (1.57-fold) (Table 1, $p < 0.05$). The T_{max_cereb} was not changed by treatment with PSC833 (Table 1).

Blood Profile and Metabolism of [^{11}C]Verapamil. The time-^{11}C radioactivity in the blood is shown in Fig. 3. The ^{11}C radioactivity in the blood fell quickly up to 3 min and then remained constant or slightly increased. Treatment with PSC833 did not affect the blood ^{11}C radioactivity profile (two-way ANOVA). The blood AUC (AUC_{blood}) of the PSC833 treatment group was similar to that of the control group (Table 1).

A chromatogram of the HPLC analysis of [^{11}C]verapamil, with or without treatment with PSC833, is shown in Fig. 4A. The retention time of verapamil was approximately 7 to 8 min. The fraction of intact verapamil decreased with time (Fig. 4B). At 10 min after administration, on average, approximately 25% of the radioactivity in plasma was the metabolite of [^{11}C]verapamil in the control group and intact verapamil represented approximately 50% of the radioactivity in the plasma of the control group 30 min after administration

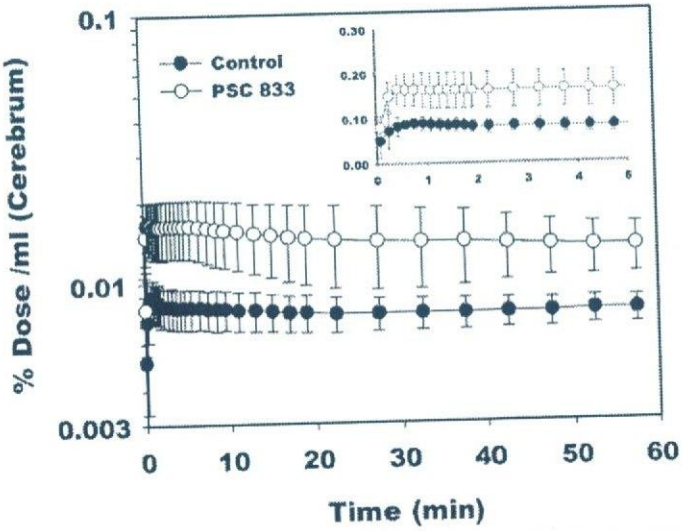

Fig. 2. The ^{11}C radioactivity time curves in cerebrum. The inset shows the detail curves in the early time period (mean ± S.D., $n = 3$). The treatment with PSC833 clearly increases the ^{11}C radioactivity in the cerebrum (two-way ANOVA, $p < 0.05$).

TABLE 1

Pharmacokinetic parameters of [^{11}C]verapamil after intravenous administration, with or without PSC833 (20 mg/kg/2 h)

The AUC_{blood} and AUC_{cereb} were calculated from 0 to 4.5 min after the administration using data shown in Figs. 2 and 3. CL_{uptake} and V_E were obtained from Figure 5. The values represent mean ± S.D. (n = 3). Data in parentheses indicate values from individual animals.

Pharmacokinetic Parameter	Control	+ PSC833 Treatment
AUC_{blood} (% dose × min/ml)	0.0567 ± 0.0145 (0.0461, 0.0733, 0.0507)	0.0535 ± 0.0331 (0.0418, 0.0279, 0.0909)
AUC_{cereb} (% dose × min/g)	0.0365 ± 0.0039 (0.0407, 0.0359, 0.0328)	0.0713 ± 0.0169* (0.0795, 0.0519, 0.0827)
C_{max_cereb} (% dose/g)	0.0105 ± 0.0006 (0.0104, 0.00989, 0.0112)	0.0166 ± 0.0033* (0.0185, 0.0128, 0.0192)
T_{max_cereb} (min)	0.58 ± 0.44 (1.08, 0.42, 0.25)	0.59 ± 0.29 (0.92, 0.42, 0.42)
CL_{uptake} (ml/g/min)	0.141 ± 0.043 (0.185, 0.139, 0.100)	0.651 ± 0.333* (0.937, 0.731, 0.285)
V_E (ml/g)	0.243 ± 0.130 (0.286, 0.0971, 0.346)	0.436 ± 0.279 (0.402, 0.731, 0.176)

* A statistically significant difference was observed (t test, $P < 0.05$).

(Fig. 4B). Treatment with PSC833 slightly increased the metabolite fraction in plasma (Fig. 4B; two-way ANOVA, $p < 0.05$). The inset in Fig. 3 shows the time-activity curves of intact [^{11}C]verapamil in plasma. The plasma radioactivity profile of intact [^{11}C]verapamil was not affected by treatment with PSC833 (two-way ANOVA).

The Brain Uptake Clearance of [^{11}C]Verapamil and Effect of PSC833. Integration plots of the control and PSC833 treatment studies of the three monkeys are shown in Fig. 5, A through C. The integration plots were linear over a short period, which varied from 1 min to 4.5 min, depending on the subject and with or without PSC833 treatment. During this period, the metabolite of [^{11}C]verapamil accounted for less than 12.5% ^{11}C radioactivity. The initial brain uptake of the control group was 0.141 ml/g/min (0.141 ± 0.043, mean ± S.D.), and this was increased after PSC833 treatment (0.651 ± 0.333 ml/g brain/min, mean ± S.D., $p < 0.05$). The V_E was not changed by PSC833 treatment (Table 1). The AUC_{cereb}/AUC_{blood} ratio of ^{11}C radioactivity was increased 2.31-fold in the presence of PSC833.

Discussion

In this study, we evaluated the P-gp function at the BBB in vivo using PET with [^{11}C]verapamil. Recently, the use of imaging techniques, such as single photon emission-computed tomography and PET using [^{11}C]colchicine, [^{11}C]carvedilol, [^{18}F]paclitaxel, and [^{64}Cu]complexes and [^{68}Ga]complexes and [^{99m}Tc]complexes, has been suggested for the noninvasive evaluation of P-gp function in vivo (Elsinga et al., 2004). Among these compounds, [^{11}C]verapamil is a well characterized PET ligand for evaluating P-gp function at the BBB (Hendrikse et al., 1998, 1999), and verapamil can be easily labeled with ^{11}C using commercially available norverapamil (Wegman et al., 2002).

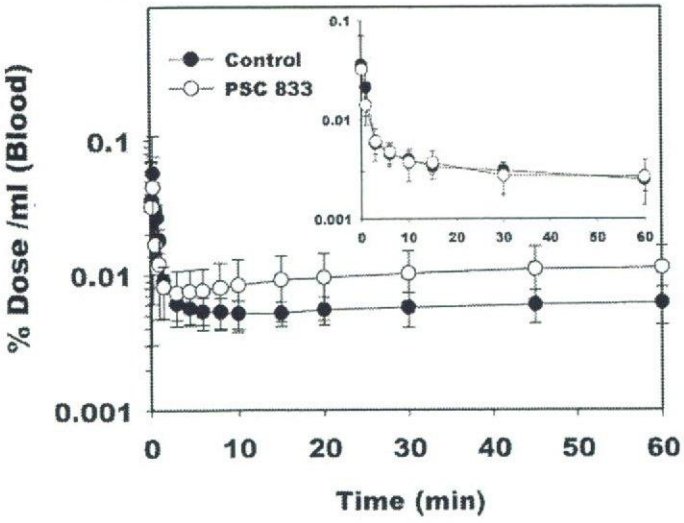

Fig. 3. The [^{11}C]radioactivity and intact (inset) [^{11}C]verapamil activity-time curves in cerebrum and blood. The time-^{11}C radioactivity and intact [^{11}C]verapamil activity curves in blood are similar for both the control and PSC833 treatment groups (mean ± S.D., n = 3).

After intravenous administration of [^{11}C]verapamil, it was rapidly distributed in the brain over a short period and then was eliminated slowly (Fig. 2). Apparently, the ^{11}C radioactivity reached a distributional pseudoequilibrium within a short period (Fig. 3). This is similar to earlier results obtained in rats (Hendrikse et al., 1999). The uptake of ^{11}C radioactivity into the cerebrum increased after PSC833 treatment (Figs. 1 and 2). PSC833 treatment increased the AUC_{cereb} and C_{max_cereb} of ^{11}C radioactivity compared with the values obtained in the control group (Table 1). These data indicate that the efflux transport by P-gp affects the initial brain uptake and that the inhibition of P-gp-mediated transport increases the brain uptake of P-gp substrates (Kusuhara et al., 1997; Dagenais et al., 2000) and supports recent human brain PET study using [^{11}C]verapamil, which was published during the revision process of this manuscript (Sasongko et al., 2005).

The blood concentration-time profile of the ^{11}C radioactivity was biphasic, exhibiting a rapid reduction within minutes followed by an increase in the ^{11}C radioactivity (Fig. 3). The increase at later time points was more marked in the PSC833-treated group than in the control group. The ^{11}C radioactivity in the blood specimens includes unchanged [^{11}C]verapamil and its metabolites (Fig. 4A). Approximately 75% of the ^{11}C radioactivity was unchanged [^{11}C]verapamil during the initial 10 min, and the fraction of the unchanged form in the blood specimens rapidly decreased (Fig. 4B). This observation is consistent with the previous reports of verapamil metabolism in humans (Kroemer et al., 1993; von Richter et al., 2000; von Richter et al., 2001) and monkeys (Link, 2003), whereas low levels of the metabolite of [^{11}C]verapamil during PET studies have been reported in rodents (Hendrikse et al., 1998, 1999). Because the increase at later time points was not observed in the blood concentration-time profile of unchanged [^{11}C]verapamil (Fig. 3, inset), it is likely that the increase is due to the accumulation of metabo-

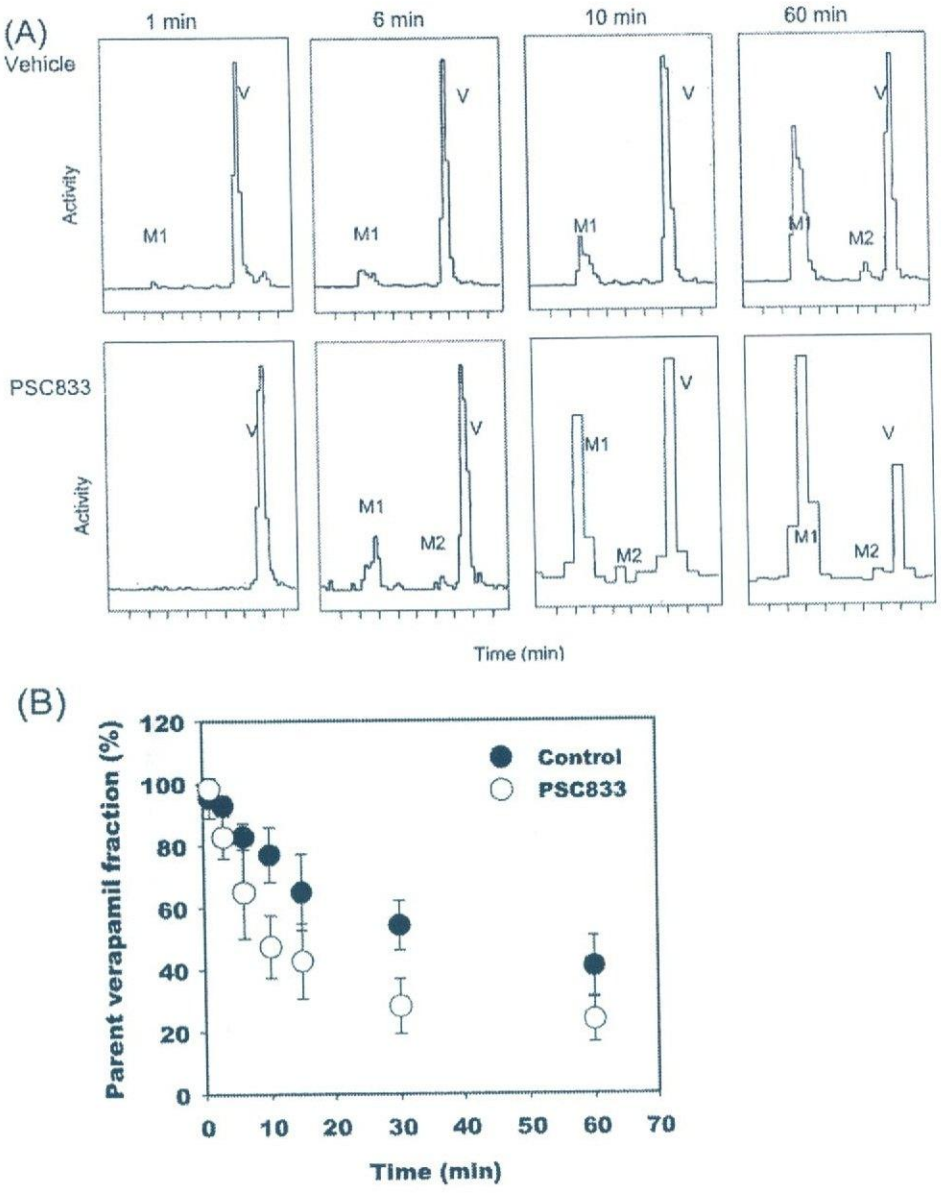

Fig. 4. A, typical chromatograms of plasma samples at 1, 6, 10, and 60 min after intravenous administration of [^{11}C]verapamil, with or without PSC833. B, parent [^{11}C]verapamil fraction of the ^{11}C radioactivity in plasma. The parent verapamil was detected at approximately 7 to 8 min (V). HPLC analysis suggested that there are at least two metabolites (M1, M2) of verapamil after intravenous administration. The parent fraction of verapamil in plasma fell rapidly with time. At 10 min after administration, on average, approximately 75% of the radioactivity in plasma was due to the parent verapamil in the control group and the parent verapamil represented approximately 50% of the radioactivity in the plasma of the control group 30 min after administration (mean ± S.D., n = 3).

lites in the blood from the peripheral tissues. Since PSC833 is known to be a fairly specific P-gp inhibitor with a low degree of metabolic inhibition (Kawahara et al., 2000) and metabolites of verapamil are also substrates of P-gp with a range of specificities (Pauli-Magnus et al., 2000), PSC833 treatment may cause a delay in the elimination of metabolized verapamil, resulting in marked plasma accumulation of metabolites.

Because we could not separate metabolites from parent verapamil in brain, there is a possibility that different parent/metabolite ratio might exist in the brain compared with blood. To deal with this extensive metabolism of [^{11}C]verapamil, we used the initial PET data (~0–4.5min) to avoid any bias from metabolites. Integration plot analysis has been used to obtain a tissue-specific uptake clearance. The initial PET scan data (from 0 to ~1–4.5 min, depending on the subjects) was enough to calculate the initial uptake clearance, during which no extensive metabolism of verapamil was observed (Fig. 4). Figure 5 shows the integration plot of the blood versus tissue time-activity curves in three monkeys (Fig. 5). The CL_{uptake} calculated from the slope of the integration plot increased after treatment with PSC833. This indicates the modulation of P-gp function at the BBB by PSC833 (Table 1) (Kusuhara et al., 1997; Song et al., 1999). The initial brain uptake clearance of [^{11}C]verapamil is a sensitive parameter for P-gp function at the BBB. However, the magnitude of the increase observed in PSC833-treated monkeys was not as high as that observed in P-gp knockout mice. This may be explained by incomplete inhibition of P-gp activity by PSC833, variable brain concentration of PSC833 in monkey, and, partly, a species difference in P-gp expression and/or intrinsic efflux transport activity. In fact, PSC833 treatment does not fully inhibit P-gp function at the BBB in mice (Kusuhara et al., 1997). Interestingly, recent human [^{11}C]verapamil PET study in the presence of cyclosporin A showed a similar degree of increase in the brain distribution of verapamil by P-gp inhibition. In this study, the AUC_{cereb}/AUC_{blood} ratio of ^{11}C radioactivity was increased 1.88-fold in the presence of cyclosporin A, which was consistent with the present study (2.31-fold) (Sasongko et al., 2005). This supports the belief that the species difference in the role of P-gp

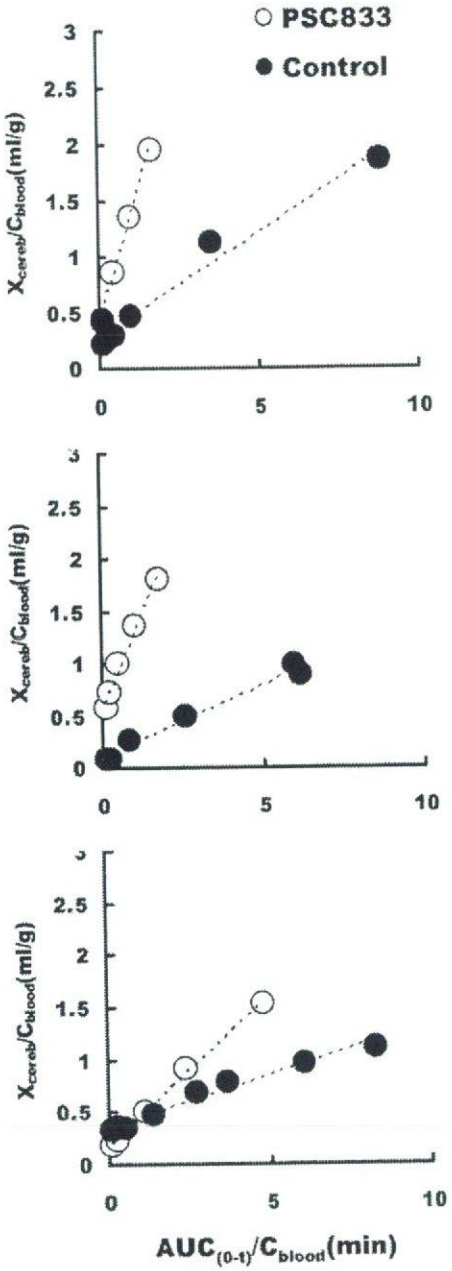

Fig. 5. Integration plot of the brain uptake of [^{11}C]verapamil for the three monkeys (A, B, and C). The initial brain uptake of the control group was increased after treatment with PSC833 (t test, $p < 0.05$, $n = 3$). The V_E was not changed by PSC833 treatment.

at the BBB may not be very significant between humans and monkeys and suggests the feasibility of a PET study using monkeys to provide information on the human BBB. Unlike the slope, the y-intercept of the plot was insensitive to the PSC833 treatment (Table 1). The y-intercept represents the initial distribution volume, including the vascular space and rapid adsorption/binding to the vascular surface, which can achieve rapid equilibrium with the blood compartment. Because the initial distribution volume is greater than the vascular space in the brain, estimated to be 35μl/g brain in 15 adult rhesus monkeys (Eichling et al., 1975), it seems that the adsorption/binding of [^{11}C]verapamil to the vascular surface occurs within a short period. The use of integration plot analysis helps in the quantitative investigation of P-gp function at the BBB without any interference from the rapid and extensive metabolism of [^{11}C]verapamil, which makes it inappropriate to use common graphical methods that need data obtained from long-term sampling (Logan, 2003).

In conclusion, we have been able to evaluate P-gp function at the BBB in nonhuman primates, using [^{11}C]verapamil as a PET ligand and integration plot method. P-gp at the BBB has attracted much interest from a clinical point of view; i.e., drug-drug interactions and the effects of genetic polymorphisms. Therefore, in future, PET studies using [^{11}C]verapamil will be a powerful tool for evaluating P-gp function at the BBB in a noninvasive manner.

Acknowledgments

We thank the members of the Cyclotron Unit and Radiopharmaceutical and Radiopharmacological Section for operation of the cyclotron and the production of radioisotopes, Novartis Pharm AG for its kind gift of PSC833, and Eisai Co. Ltd. for its kind gift of norverapamil.

References

Bart J, Willemsen AT, Groen HJ, van der Graaf WT, Wegman TD, Vaalburg W, de Vries EG, and Hendrikse NH (2003) Quantitative assessment of P-glycoprotein function in the rat blood-brain barrier by distribution volume of [^{11}C]verapamil measured with PET. *Neuroimage* **20**:1775–1782.

Dagenais C, Rousselle C, Pollack GM, and Scherrmann JM (2000) Development of an in situ mouse brain perfusion model and its application to mdr1a P-glycoprotein-deficient mice. *J Cereb Blood Flow Metab* **20**:381–386.

Eichling JO, Raichle ME, Grubb RL Jr, Larson KB, and Ter-Pogossian MM (1975). In vivo determination of cerebral blood volume with radioactive oxygen-15 in the monkey. *Circ Res* **37**:707–714.

Elsinga PH, Hendrikse NH, Bart J, Vaalburg W, and van Waarde A (2004) PET studies on P-glycoprotein function in the blood-brain barrier: how it affects uptake and binding of drugs within the CNS. *Curr Pharm Des* **10**:1493–1503.

Hendrikse N, Schinkel A, de Vries E, Fluks E, Van der Graaf W, Willemsen A, Vaalburg W, and Franssen E (1998) Complete in vivo reversal of P-glycoprotein pump function in the blood- brain barrier visualized with positron emission tomography. *Br J Pharmacol* **124**:1413–1418.

Hendrikse NH, de Vries EG, Eriks-Fluks L, van der Graaf WT, Hospers GA, Willemsen AT, Vaalburg W, and Franssen EJ (1999) A new in vivo method to study P-glycoprotein transport in tumors and the blood-brain barrier. *Cancer Res* **59**: 2411–2416.

Hirrlinger J, Konig J, and Dringen R (2002) Expression of mRNAs of multidrug resistance proteins (Mrps) in cultured rat astrocytes, oligodendrocytes, microglial cells and neurones. *J Neurochem* **82**:716–719.

Kawahara I, Kato Y, Suzuki H, Achira M, Ito K, Crespi CL, and Sugiyama Y (2000) Selective inhibition of human cytochrome P450 3A4 by *N*-[2(*R*)-hydroxy-1(*S*)-indanyl]-5-[2(*S*)-(1,1-dimethylethylaminocarbonyl)-4-[(furo[2, 3-b]pyridin-5-yl)methyl]piperazin-1-yl]-4(*S*)-hydroxy-2(*R*)-phenylmethylpentanamide and P-glycoprotein by valspodar in gene transfectant systems. *Drug Metab Dispos* **28**: 1238–1243.

Kim DC, Sugiyama Y, Satoh H, Fuwa T, Iga T, and Hanano M (1988) Kinetic analysis of in vivo receptor-dependent binding of human epidermal growth factor by rat tissues. *J Pharm Sci* **77**:200–207.

Kortekaas R, Leenders KL, van Oostrom JC, Vaalburg W, Bart J, Willemsen AT, and Hendrikse NH (2005) Blood-brain barrier dysfunction in parkinsonian midbrain in vivo. *Ann Neurol* **57**:176–179.

Kroemer HK, Gautier JC, Beaune P, Henderson C, Wolf CR, and Eichelbaum M (1993) Identification of P450 enzymes involved in metabolism of verapamil in humans. *Naunyn-Schmiedeberg's Arch Pharmacol* **348**:332–337.

Kusuhara H and Sugiyama Y (2001) Efflux transport systems for drugs at the blood-brain barrier and blood-cerebrospinal fluid barrier (part 1). *Drug Discov Today* **6**:150–156.

Kusuhara H, Suzuki H, Terasaki T, Kakee A, Lemaire M, and Sugiyama Y (1997) P-glycoprotein mediates the efflux of quinidine across the blood-brain barrier. *J Pharmacol Exp Ther* **283**:574–580.

Lam FC, Liu R, Lu P, Shapiro AB, Renoir JM, Sharom FJ, and Reiner PB (2001) β-Amyloid efflux mediated by p-glycoprotein. *J Neurochem* **76**:1121–1128.

Link JM (2003) PET imaging of in vivo transporter and receptor activity, in *AAPS Workshop on Drug Transport: From the Bench to the Bedside*, Wyndham Peachtree Conference Center, Peachtree City, GA.

Logan J (2003) A review of graphical methods for tracer studies and strategies to reduce bias. *Nucl Med Biol* **30**:833–844.

Lo Y, Liu F, and Cherng J (2001) Effect of PSC 833 liposomes and Intralipid on the transport of epirubicin in Caco-2 cells and rat intestines. *J Control Release* **76**:1–10.

Maeda J, Suhara T, Ogawa M, Okauchi T, Kawabe K, Zhang MR, Semba J, and Suzuki K (2001) In vivo binding properties of [carbonyl-^{11}C]WAY-100635: effect of endogenous serotonin. *Synapse* **40**:122–129.

Obayashi S, Suhara T, Kawabe K, Okauchi T, Maeda J, Akine Y, Onoe H, and Iriki A (2001) Functional brain mapping of monkey tool use. *Neuroimage* **14**:853–861.

Pardridge WM (1988) Recent advances in blood-brain barrier transport. *Annu Rev Pharmacol Toxicol* **28**:25–39.

Pauli-Magnus C, von Richter O, Burk O, Ziegler A, Mettang T, Eichelbaum M, and Fromm MF (2000) Characterization of the major metabolites of verapamil as substrates and inhibitors of P-glycoprotein. *J Pharmacol Exp Ther* **293**:376–382.

Reese TS and Karnovsky MJ (1967) Fine structural localization of a blood-brain barrier to exogenous peroxidase. *J Cell Biol* **34**:207–217.

Rodriguez M, Ortega I, Soengas I, Suarez E, Lukas JC, and Calvo R (2004) Effect of P-glycoprotein inhibition on methadone analgesia and brain distribution in the rat. *J Pharm Pharmacol* **56**:367–374.

Sadeque AJ, Wandel C, He H, Shah S, and Wood AJ (2000) Increased drug delivery to the brain by P-glycoprotein inhibition. *Clin Pharmacol Ther* **68**:231–237.

Sasongko L, Link JM, Muzi M, Mankoff DA, Yang X, Collier AC, Shoner SC, and Unadkat JD (2005) Imaging P-glycoprotein transport activity at the human blood-brain barrier with positron emission tomography. *Clin Pharmacol Ther* **77**:503–514.

Schinkel AH, Smit JJ, van Tellingen O, Beijnen JH, Wagenaar E, van Deemter L, Mol CA, van der Valk MA, Robanus-Maandag EC, te Riele HP, et al. (1994) Disruption of the mouse mdr1a P-glycoprotein gene leads to a deficiency in the blood-brain barrier and to increased sensitivity to drugs. *Cell* **77**:491–502.

Siddiqui A, Kerb R, Weale ME, Brinkmann U, Smith A, Goldstein DB, Wood NW, and Sisodiya SM (2003) Association of multidrug resistance in epilepsy with a polymorphism in the drug-transporter gene ABCB1. *N Engl J Med* **348**:1442–1448.

Song S, Suzuki H, Kawai R, and Sugiyama Y (1999) Effect of PSC 833, a P-glycoprotein modulator, on the disposition of Vincristine and digoxin in rats. *Drug Metab Dispos* **27**:689–694.

Takei M, Kida T, and Suzuki K (2001) Sensitive measurement of positron emitters eluted from HPLC. *Appl Radiat Isot* **55**:229–234.

Tamai I and Tsuji A (2000) Transporter-mediated permeation of drugs across the blood-brain barrier. *J Pharm Sci* **89**:1371–1388.

Tan NC, Heron SE, Scheffer IE, Pelekanos JT, McMahon JM, Vears DF, Mulley JC, and Berkovic SF (2004) Failure to confirm association of a polymorphism in ABCB1 with multidrug-resistant epilepsy. *Neurology* **63**:1090–1092.

Vogelgesang S, Cascorbi I, Schroeder E, Pahnke J, Kroemer HK, Siegmund W, Kunert-Keil C, Walker LC, and Warzok RW (2002) Deposition of Alzheimer's β-amyloid is inversely correlated with P-glycoprotein expression in the brains of elderly non-demented humans. *Pharmacogenetics* **12**:535–541.

von Richter O, Eichelbaum M, Schonberger F, and Hofmann U (2000) Rapid and highly sensitive method for the determination of verapamil, [2H7]verapamil and metabolites in biological fluids by liquid chromatography-mass spectrometry. *J Chromatogr B Biomed Sci Appl* **738**:137–147.

von Richter O, Greiner B, Fromm MF, Fraser R, Omari T, Barclay ML, Dent J, Somogyi AA, and Eichelbaum M (2001) Determination of in vivo absorption, metabolism and transport of drugs by the human intestinal wall and liver with a novel perfusion technique. *Clin Pharmacol Ther* **70**:217–227.

Watanabe M, Okada H, Shimizu K, Omura T, Yoshikawa E, Kosugi T, Mori S, and Yamashita T (1997) A high resolution animal PET scanner using compact PS-PMT detectors. *IEEE Trans Nucl Sci* **44**:1277–1282.

Wegman TD, Maas B, Elsinga PH, and Vaalburg W (2002) An improved method for the preparation of [^{11}C]verapamil. *Appl Radiat Isot* **57**:505–507.

Address correspondence to: Dr. Tetsuya Suhara, Brain Imaging Project, National Institute of Radiological Sciences, 9-1, Anagawa 4-Chome, Inage-ku, Chiba 263-8555, Japan. E-mail: suhara@nirs.go.jp

Quantitative Analysis of ^{11}C-Verapamil Transfer at the Human Blood–Brain Barrier for Evaluation of P-glycoprotein Function

Yoko Ikoma[1], Akihiro Takano[1], Hiroshi Ito[1], Hiroyuki Kusuhara[2], Yuichi Sugiyama[2], Ryosuke Arakawa[1,3], Toshimitsu Fukumura[4], Ryuji Nakao[4], Kazutoshi Suzuki[4], and Tetsuya Suhara[1]

[1]Department of Molecular Neuroimaging, Molecular Imaging Center, National Institute of Radiological Sciences, Chiba, Japan; [2]Department of Molecular Pharmacokinetics, Graduate School of Pharmaceutical Sciences, University of Tokyo, Tokyo, Japan; [3]Department of Neuropsychiatry, Nippon Medical School, Tokyo, Japan; and [4]Department of Radiochemistry, Molecular Imaging Center, National Institute of Radiological Sciences, Chiba, Japan

P-glycoprotein in the blood–brain barrier (BBB) has been found to be associated with several types of neurologic damage. ^{11}C-Verapamil has been used for in vivo imaging of P-glycoprotein function in the BBB by PET, but metabolites in plasma complicate the quantitative analysis of human studies. In this study, we validated the quantification methods of ^{11}C-verapamil transfer from plasma to the brain in humans. **Methods:** The transfer rate constant from plasma to the brain, K_1, was estimated by nonlinear least squares (NLS) with a 2-input compartment model, including the permeation of the main metabolite in plasma at the BBB, and with a 1-input compartment model using only 15-min data that contained little metabolite in plasma. K_1 was also estimated by graphical analysis of an integration plot that uses only early-time data, before the appearance of metabolites, and the estimated K_1 was compared with that obtained by the NLS method. In the simulation study, the reliability of parameter estimates in the graphical analysis method was investigated for various values of rate constants, time ranges of parameter estimations, and noise levels. **Results:** ^{11}C-Verapamil in plasma gradually converted to its metabolites, and about 45% of the radioactivity in the plasma specimen was associated with ^{11}C-verapamil metabolites at 30 min after injection. Although K_1 estimated from graphical analysis was slightly smaller than that by NLS, there was strong correlation among the K_1 values obtained by these 3 methods. In the simulation study, for graphical analysis, the differences between the true and mean of K_1 estimates became larger and the coefficient of variation (COV) of K_1 estimates became smaller as the end time of linear regression became later. The COV of graphical analysis was almost equal to that of NLS with the 1-input compartment model. **Conclusion:** The transfer of ^{11}C-verapamil from plasma to the brain was able to be quantitatively estimated by graphical analysis because this method can provide K_1 from the data of the initial few minutes without considering the effect of the metabolites in plasma.

Received Feb. 8, 2006; revision accepted May 10, 2006.

For correspondence or reprints contact: Hiroshi Ito, MD, PhD, Department of Molecular Neuroimaging, Molecular Imaging Center, National Institute of Radiological Sciences, 4-9-1, Anagawa, Inage-ku, Chiba, 263-8555, Japan.
E-mail: hito@nirs.go.jp

Key Words: ^{11}C-verapamil; PET; P-glycoprotein; blood–brain barrier; transfer rate constant

J Nucl Med 2006; 47:1531–1537

P-glycoprotein (P-gp) is found at cell membranes of various organs, and functions as an efflux pump hampering the invasion of toxic compounds into the cells (*1–4*). P-gp is also expressed at the blood–brain barrier (BBB), a functional barrier between blood and brain interstitial space formed by a continuous endothelial lining of cerebral capillaries, and plays indispensable roles as one of the barrier functions in BBB (*5–8*). In addition to its pharmacologic importance, P-gp in BBB was recently found to be associated with several neurologic disorders (*9,10*).

^{11}C-Verapamil has been used for in vivo neuroimaging of the brain by PET, representing a potent tool for imaging the function of P-gp (*11–14*). Some investigators analyzed the kinetics of ^{11}C-verapamil by the distribution volume (DV) estimated from the graphical analysis developed by Logan et al. (*15*) in rodents, reporting that the DV was increased by the pretreatment of cyclosporin A (CsA), a P-gp inhibitor (*16,17*). In a human study, Sasongko et al. demonstrated that the ratio of the area under the curve of brain to that of blood was increased in the presence of CsA (*18*), and Kortekaas et al. reported that the uptake of ^{11}C-verapamil as evaluated by the DV with the graphical analysis of Logan et al. was elevated in the midbrain of Parkinson's disease patients as compared with control subjects (*19*). On the other hand, Lee et al. evaluated the transfer of ^{11}C-verapamil from blood to brain with the graphical analysis using early-time data, the so-called integration plot, in rhesus monkeys with or without treatment of a P-gp inhibitor, PSC833, demonstrating that the brain uptake of ^{11}C-verapamil was increased after the PSC833 treatment (*20*). Moreover, Muzi et al. estimated the rate constant of ^{11}C-verapamil transfer to the brain, K_1, with 1- and 2-tissue compartment models in healthy

volunteers, reporting that K_1 increased in the presence of the P-gp inhibitor CsA (*21*). This means that the initial brain uptake of ^{11}C-verapamil can be an indicator of the P-gp activity at the BBB. However, Sasongko et al. reported that the plasma radioactivity of verapamil was approximately 35%, that of the main metabolite D-617 was 20% at 45 min, and that D-617 and several other minor metabolites might contribute to the image (*18*). Although these metabolites in plasma complicate the quantitative analysis, validation of these kinetic analysis methods for ^{11}C-verapamil has not been sufficiently confirmed in humans.

In this study, we evaluated the quantitative analysis methods to estimate the transfer of ^{11}C-verapamil from plasma to the brain in healthy volunteers, and the reliability of the estimated parameters was investigated by computer simulation.

MATERIALS AND METHODS

Subjects

Ten subjects (age range, 20–31 y; mean age ± SD, 23.8 ± 3.3 y) participated in this study. All volunteers were free of any somatic, neurologic, or psychiatric disorders, and they had no history of current or previous drug abuse. This study was approved by the Ethics and Radiation Safety Committees of the National Institute of Radiological Sciences, Chiba, Japan, and written informed consent was obtained from each subject.

Radioligand

^{11}C-Verapamil was synthesized from norverapamil (Eisai Co. Ltd.) as described previously (*22*).

PET

PET scans were performed using an ECAT EXACT 47 scanner (CTI/Siemens), which provides 47 planes and a 16.2-cm axial field of view. A transmission scan with a 3-rod source of ^{68}Ge-^{68}Ga was followed by a dynamic 60-min scan (15 s × 8, 30 s × 4, 60 s × 2, 120 s × 1, 240 s × 4, 360 s × 6) with a bolus injection of 629.0–856.9 MBq (mean ± SD, 746.3 ± 58.2 MBq) of ^{11}C-verapamil. The specific radioactivities were 31.0–99.3 GBq/μmol (mean ± SD, 48.1 ± 20.6 GBq/μmol) at the time of injection. The PET data were acquired in 2-dimensional mode and the data were reconstructed by filtered backprojection using a ramp filter with a cutoff frequency of 0.5.

MRI was performed with a Gyroscan NT scanner (1.5 T) (Phillips Medical Systems) to obtain T1-weighted images of the brain.

The PET images were coregistered to MR images, and regions of interest (ROIs) were defined over the frontal, temporal, parietal, and occipital cortices, and the cerebellum with a template-based method as described by Yasuno et al. (*23*).

Arterial Blood Sampling

To obtain the arterial input function, an automated blood sampling system was used during the first 5 min of each PET measurement (*24*). The concentration of radioactivity in arterial blood was measured every second. At the same time, arterial blood samples were taken manually and their radioactive concentrations were measured 26 times during the scan. Each manually taken blood sample was centrifuged to obtain plasma and blood cell fractions, and the concentration of radioactivity in the plasma was measured. Radioactivity between PET and blood was calibrated with a cylinder phantom and ^{18}F solution. Plasma metabolites were analyzed as follows: For the plasma fractions at 2, 4, 7, 12, 19, 29, 42, and 59 min after injection, acetonitrile was added and then centrifuged. The supernatant was analyzed for radioactive components using a high-performance liquid chromatography system (PU-610A series; GL Sciences) with a coupled bismuth germanate positron detector (*25*) to measure plasma ^{11}C-verapamil metabolites. Isocratic elution was performed with a reversed-phase semipreparative Waters μBondpak C_{18} column (7.8 mm [inner diameter] × 300 mm). The mobile phase consisted of a mixture of acetonitrile and 0.1 mol/L ammonium acetate (70:30, v/v). The percentage of parent radioactivity was determined from the activity of the parent verapamil with respect to the total activity in the chromatogram.

Data Analysis

2-Input Compartment Model. The rate constants between plasma and tissue were estimated both for unmetabolized ^{11}C-verapamil and for the main metabolite with a 2-input, 2-tissue compartment model including transfer of the metabolite from plasma to brain (Fig. 1) (*26,27*). K_1 describes the rate constant for transfer of ^{11}C-verapamil from plasma to brain, k_2 describes the rate constant for transfer of ^{11}C-verapamil from brain to plasma, and K_1^M and k_2^M represent the transfer of the main metabolite between plasma and brain. The fraction of unchanged ^{11}C-verapamil in the total plasma radioactivity was fitted by a 2-exponential expression (*28*), $f = a \times \exp(-bt) + (1 - a) \times \exp(-ct)$, where f is the fraction of unchanged ^{11}C-verapamil, and a, b, and c are the estimated parameters. A plasma curve of unchanged ^{11}C-verapamil used as input function C_p was generated by the product of the plasma activity and the fraction curves of unchanged ^{11}C-verapamil. Meanwhile, the fraction of the main metabolite in total plasma radioactivity was fitted by $f' = 1 - \{a' \times \exp(-b't) + (1 - a') \times \exp(-c't)\}$, where f′ is the fraction of the main metabolite, and a′, b′, and c′ are the estimated parameters. A plasma curve of the

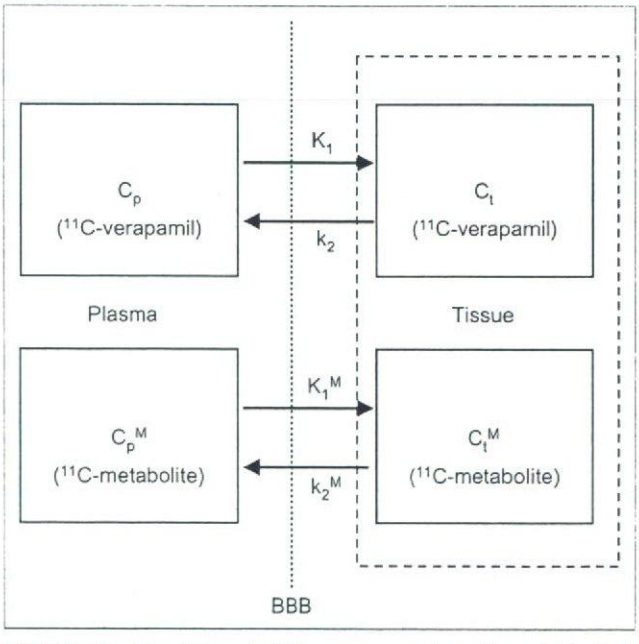

FIGURE 1. The 2-input, 2-tissue compartment model including transfer of metabolite in plasma to tissue.

main metabolite used as input function C_p^M was generated by the product of the plasma activity and the metabolite fraction curves. In this model, 5 parameters (K_1, k_2, K_1^M, k_2^M, blood volume [BV]) were estimated by nonlinear least squares (NLS) with iteration of the Modified Marquardt algorithm without weighting and without constraints. Parameter estimates were considered invalid if DV [$= K_1/k_2$] and DV^M [$= K_1^M/k_2^M$ were outside the range $0.0 < DV, DV^M < 5.0$.

1-Input Compartment Model. Rate constants between plasma and tissue—that is, K_1 and k_2—were also estimated with a 1-input, 1-tissue compartment model including only the transfer of unmetabolized ^{11}C-verapamil. In this model, a plasma curve of unchanged ^{11}C-verapamil was used as input function C_p, and 3 parameters (K_1, k_2, BV) were estimated by NLS in the same way as in the 2-input compartment model. NLS fitting was performed for both 60-min data and 15-min data.

Uptake Estimates with Graphical Analysis. The rate constant of transfer from plasma to brain was estimated by the graphical analysis method with integration of plasma input versus tissue (integration plot) (*20,29*). In the 1-input, 1-tissue compartment model, the radioactivity concentration in the brain is given by:

$$C_b(t) = K_1 \int_0^t C_p(s)ds - k_2 \int_0^t C_b(s)ds, \qquad \text{Eq. 1}$$

where C_p and C_b are the radioactivity concentration of unchanged ^{11}C-verapamil in plasma and brain, respectively; K_1 is the transfer rate constant from plasma to brain; and k_2 is the efflux rate constant from the brain. In the early phase after administration of tracer, as efflux from the brain and metabolites in plasma is negligible, the second term is small enough to eliminate, and radioactivity concentration in the brain can be described by:

$$C_b(t) = K_1 \int_0^t C_p(s)ds. \qquad \text{Eq. 2}$$

When a BV component is considered, measured radioactivity concentration in the ROI is given by:

$$C_t(t) = (1 - BV)C_b(t) + BV \times C_w(t), \qquad \text{Eq. 3}$$

where $C_w(t)$ is the radioactivity concentration in whole blood, and BV is the blood volume. From Equations 2 and 3, K_1 can be obtained by linear regression from the equation:

$$\frac{C_t(t)}{C_w(t)} = (1 - BV)K_1 \times \frac{\int_0^t C_p(s)ds}{C_w(t)} + BV \quad for\ t < t_e, \qquad \text{Eq. 4}$$

where t_e is the end-time-point of linear regression in which efflux from the brain is assumed to be negligible. In this study, points of the first frame were excluded from linear regression to eliminate the large variation in time–activity curves of the brain, and $(1 - BV)K_1$ and BV were estimated as slope and intercept, respectively, by linear regression using points of 9 frames from the second frame (mean time point = 22.5 s) to the 10th frame (mean time point = 165 s) after the injection. K_1 estimated from the integration plot was compared with that from NLS with 2-input or 1-input compartment models.

Analysis of human data was implemented using MATLAB (The MathWorks) or PMOD (PMOD Technologies).

Simulation Study

The reliability of K_1 estimated with the integration plot was evaluated by computer simulation. Because there was little metabolite in plasma during the initial 12 min used in the evaluation of the integration plot, simulated time–activity curves were generated according to the 1-input, 1-tissue compartment model. Time–activity curves were simulated with measured input function for various rate constants (k values: K_1 = 0.03, 0.05, and 0.07; DV = 0.4, 0.7, and 1.0; BV = 0.05). The noise ratio for each frame was determined according to the collected total count of the frame (*30,31*). Noise was generated with random numbers based on gaussian distribution and added to the nondecaying tissue activity for each frame. In this simulation study, the noise level was adjusted to be 1%, 3%, and 5% at the 16th frame (mean time point = 10 min) of the time–activity curve with K_1 = 0.05, DV = 0.7, and 1,000 noisy datasets were generated for each k value and noise level. In these noise-added time–activity curves, K_1 was estimated by the integration plot with points from 15 s to 1, 2, 3, 5, 8, and 12 min, and the mean and the coefficient of variation (COV; SD/mean [%]) of estimated K_1 in 1,000 runs were evaluated for each.

The simulations were performed on Dr.View (Asahi Kasei Information Systems Co.).

RESULTS

PET Studies

The ratios of unchanged ^{11}C-verapamil and the main and minor metabolites in total plasma radioactivity are shown in Figure 2. The ratio of unchanged ^{11}C-verapamil was about 94% at 7 min, 83% at 12 min, 55% at 30 min, and 35% at 60 min.

The shape of the time–activity curve was similar for all regions, and measured time–activity curves of 60 min were

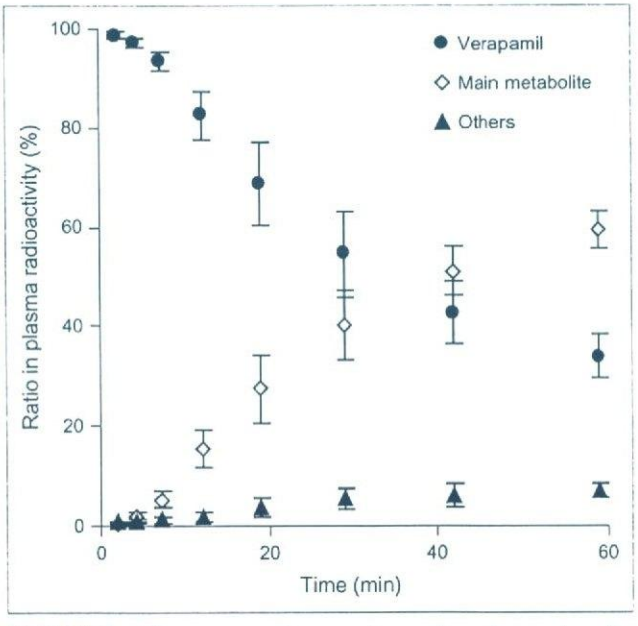

FIGURE 2. Time curve of percentage of unchanged radioligand and metabolites in total plasma radioactivity using ^{11}C-verapamil in 10 subjects.

well described by the 2-input compartment model, taking into account the transfer from the metabolite in plasma to brain (Fig. 3A). The 1-tissue compartment model was not sufficient to describe the measured time–activity curves at 60 min for all regions of the brain (Fig. 3B), and this model was able to fit the measured time–activity curves up to 15 min (Fig. 3C). The estimated rate constants of each region are listed in Table 1. In the 2-input compartment model, K_1 ranged from 0.046 (temporal) to 0.050 (occipital), K_1^M ranged from 0.057 (occipital) to 0.071 (temporal), and k_2^M ranged from 0.068 (occipital) to 0.11 (cerebellum). The COV of K_1^M and k_2^M were remarkably large. In the frontal cortex, the COV of K_1^M and k_2^M were 57% and 63%, respectively. In the 1-input compartment model by 15-min data, K_1 ranged from 0.046 (temporal) to 0.049 (cerebellum). In the graphical analysis, the brain and plasma concentration data up to about 3 min were approximately linear (Fig. 4). Estimated K_1 ranged from 0.043 (temporal) to 0.046 (occipital), values slightly smaller than those of NLS with the 2-input or the 1-input compartment model. There was strong correlation between the K_1 and k_2 values estimated with the 2-input compartment model for 60-min measured data and those with the 1-input compartment model for 15-min data (Figs. 5A and B). However, K_1 values estimated from the 1-input compartment model for 60-min data were about 10% smaller than those from the 2-input compartment model. Although the K_1 values estimated from the integration plot were slightly smaller than those of NLS, a strong correlation was also found between these methods (Fig. 5C).

Simulation Study

In the simulation study of the integration plot, plot points of Equation 4 began to fall from the linear line about 2 min after injection, especially in the time–activity curve with a small DV—that is, large k_2. In noise-added time–activity curves, K_1 was underestimated, and the difference between true and mean values of estimated K_1 changed according to the end time of linear regression, becoming large when the end time was late. The difference also became large when the K_1 value was large and the DV value was small, indicating that the k_2 value was large (Fig. 6). However, this underestimation was independent of the noise level. Furthermore, the COV of K_1 estimates became smaller as the end time of linear regression became later. The COV depended on the noise level, and it became larger as the noise level increased. When K_1 was 0.05, DV was 0.7, and the end time of linear regression was 3 min, the COV of K_1 estimates were 1.9% at 1% noise, 5.6% at 3% noise, and 9.3% at 5% noise. However, COV was independent of the DV value.

DISCUSSION

Effect of Metabolites in Plasma on Parameter Estimation

In the ^{11}C-verapamil study with the 60-min scan, the time–activity curve was not described by the 1-input, 1-tissue compartment model (Fig. 3). This might be explained by the existence of radioactive metabolites in plasma passing the BBB and increasing with time. It has been reported that there was little ^{11}C-metabolite in plasma and brain of rats 1 h after injection (*13,32*), whereas Lee et al. reported that the significant amount of radioactivity in plasma was associated with the form of metabolites of ^{11}C-verapamil 1 h after injection in nonhuman primates (*20*). Meanwhile, Sasongko et al. (*18*) reported that D-617 and several other minor metabolites would retain the label and that the plasma radioactivity of verapamil was approximately 35%, that of D-617 was 20% at 45 min, and that therefore these metabolites might contribute to the image as most of these unconjugated metabolites of verapamil have been shown to be substrates of P-gp with affinity similar to that of verapamil (*33*). In our human study, ^{11}C-verapamil was gradually converted to its metabolites after intravenous administration, and about 45% of the radioactivity in the plasma specimen was associated with ^{11}C-verapamil metabolites at 30 min after injection (Fig. 2), a

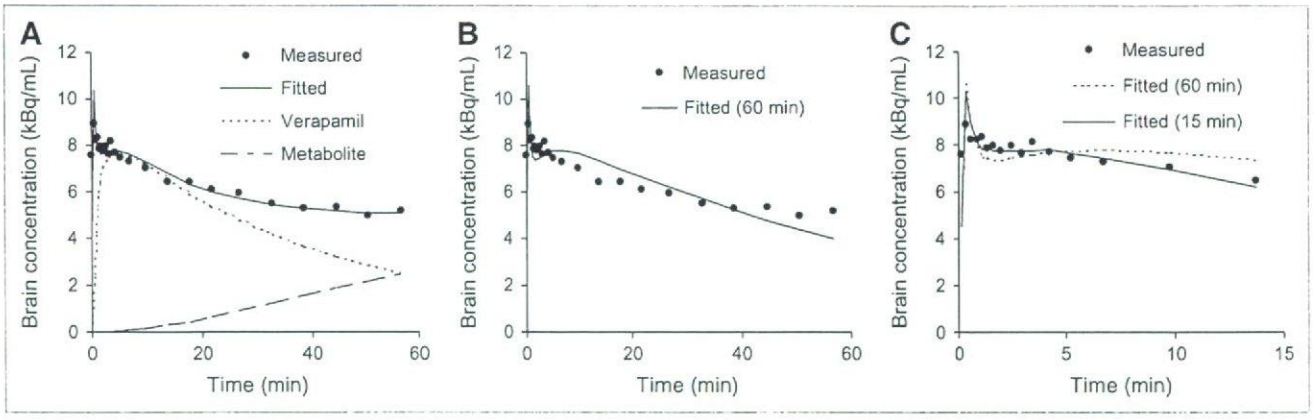

FIGURE 3. Measured time–activity curve and fitting result with 2-input compartment model (A), with 1-input compartment model using measured data up to 60 min (B), and with 1-input compartment model using measured data up to 15 min (C) for ^{11}C-verapamil. Symbols represent measured radioactivity concentrations in temporal cortex.